KSCE Journal of Civil Engineering (2023) 27(7):2930-2939
DOI 10.1007/s12205-023-0561-7

pISSN 1226-7988, eISSN 1976-3808
www.springer.com/12205

Structural Engineering

Early Performance Evolution Tracking and Monitoring for Cement-based Piezoelectric Composites under Multiple Curing Conditions

Yu Rao[a], **Zhiming Liu**[a], **Xiaoxiao Zhu**[a], **and Jun Wang**[a]

[a]*College of Civil Engineering and Architecture, Wenzhou University, Wenzhou 325035, China*

ARTICLE HISTORY

Received 16 April 2022
Revised 1st 16 February 2023
Revised 2nd 13 March 2023
Accepted 10 April 2023
Published Online 16 May 2023

KEYWORDS

Cement
Lead zirconate titanate
Composite material
Inorganic compound
Temperature
Humidity
Curing conditions
Tracking and monitoring

ABSTRACT

Piezoelectric composites based on 0 – 3 cement have been extensively employed in structural health monitoring. Significantly, curing conditions considerably affect the forming strength of matrix materials. In order to obtain the best molding conditions of 0 – 3 cement-based piezoelectric composites, this paper studied the evolution of various parameters with time during the early molding process of 0 – 3 cement-based piezoelectric composites under different temperature and humidity conditions. The analysis indicated that the higher the temperature, which increases the forming speed of the sample, the lower the curing humidity, which decreases the current generated during the polarisation process of the sample, and longer the time required to attain the polarisation voltage. The test concluded that the curing condition of high temperature and high humidity was conducive to obtaining higher piezoelectric and dielectric properties of the sample and the piezoelectric strain constant and dielectric constant reached the maximum value at 80°C/100RH, which were 45.5 pC/N and 44.36 respectively.

1. Introduction

Piezoelectric materials, which are a new type of intelligent material, can sense external vibrations and convert them into electrical signals because of its unique characteristics, thereby exhibiting properties suitable for vibration energy collection (Yang et al., 2021; Wang et al., 2021) and sensing (Hou et al., 2017; Chai et al., 2018). Currently, the lead zirconate titanate (PZT) piezoelectric ceramic is a commonly used piezoelectric material. Traditional piezoelectric ceramics are directly employed in structural health detection and monitoring research, such as acoustic monitoring (Lu et al., 2013; Lim et al., 2017; Zhang et al., 2018; Pan et al., 2019) and impedance monitoring (Ruan, 2017; Zhang et al., 2020). However, in the field of concrete monitoring, the application of traditional piezoelectric ceramics is limited because of acoustic impedance matching, deformation coordination caused by temperature and humidity, and interface adhesion. Dong et al. (2011) combined PZT particles with cement and studied the electromechanical response of this composite. The results indicated that the acoustic impedance of cement-based piezoelectric materials is proximate to that of hardened concrete, which ensures minimum signal distortion between the two materials and maximises the signal energy transmission efficiency. Moreover, cement-based piezoelectric materials exhibit good coordination with hardened concrete and can even be embedded in concrete as aggregates. These materials comprise cement material as the matrix phase and PZT powder as the functional phase. In particular, type 0 – 3 composite phase change material (CPCM) consists of PZT particles dispersed in a three-dimensional connected cement matrix that is subsequently solidified and polarised; this material is advantageous owing to its simple structure, cost effectiveness, and high compatibility with concrete. Lezgy-Nazargah et al. (2019) investigated the performance and reliability of the fabricated sensor in response to the dynamic loads with different load patterns, and the result indicated the properties of type 0 – 3 CPCM after moulding are affected by the type of ceramics and volume ratio of ceramics to cement, and its properties can be tailored for practical engineering applications. Therefore, a study on the properties and application of 0 – 3 CPCM is essential considering its practical advantages. Compared with traditional piezoelectric

CORRESPONDENCE Xiaoxiao Zhu zxxzhuxiaoxiao@163.com College of Civil Engineering and Architecture, Wenzhou University, Wenzhou 325035, China

© 2023 Korean Society of Civil Engineers

ceramics, 0 – 3 CPCM — with a lower acoustic impedance, wider frequency band, and higher sensitivity to acoustic emission signals— offers more advantages under similar monitoring conditions (Qin et al., 2010; Lu et al., 2011). Furthermore, Lu et al. (2015) used cement-based piezoelectric composite sensors monitored the early-age hydration of mineral admixtures incorporated, and found that 0 – 3 CPCM exhibits good performance in the monitoring of the early hydration process in cement. Zhou et al. (2016) used the embedded cement-based piezoelectric ceramic sensor to detect the crack propagation of the mortar specimen under the cube splitting load, described the fracture process of the mortar specimen in the cube splitting test, and proved that the cement-based piezoelectric material has good structural damage identification ability. Pan and Huang (2020) realized the monitoring of cement mortar strength by using CPCM, and the results indicated that the CPCM sensor is easy to find an effective monitoring frequency at which the conductance decreases with the age of the cementitious materials because it has the advantage of a broader frequency bandwidth that provides higher recognizing ability than the PZT. Therefore, 0 – 3 CPCM shows better performance than traditional piezoelectric ceramics in many aspects, and has great potential in civil structure health monitoring.

Huang et al. (2007) studied the influence of the forming pressure on the preparation of type 0 – 3 CPCM. With an increase in the forming pressure, the porosity decreased, whereas the quality of CPCM products was enhanced. Moreover, Huang et al. (2009) discovered that adding a certain proportion of carbon black could effectively improve the piezoelectric strain and piezoelectric voltage constants of CPCMs. Furthermore, Gong et al. (2011) incorporated a certain number of carbon nanotubes with improved interface adhesion between cement matrix and type 0 – 3 CPCM; their strategy significantly improved the conductivity of composite materials and promoted the polarisation of materials. In addition, Pan et al. (2017) investigated the influence of the water–cement ratio on the performance of 0 – 3 CPCM, compared the piezoelectric and dielectric properties of CPCM with different PZT contents, and proposed a double-sided heating technology, which significantly improved the piezoelectric performance of polarised CPCMs. Furthermore, Hunpratub et al. (2014) found that 0 – 3 CPCM composed of larger PZT particle sizes exhibited a higher piezoelectric strain constant. However, excessively large functional phase particle sizes resulted in a loose connection between the PZT particle and substrate, whereas a loose structure attenuated the piezoelectric properties of CPCM. The aforementioned research reveals that the quality of the matrix phase significantly affects the quality of the finished CPCM product.

As the forming time of the cement matrix is generally below 72 h (Huang et al., 2007; Gong et al., 2009; Huang et al., 2009), studies on 0 – 3 CPCM have primarily focused on directly measuring or using the sample after 72 h of hydration. However, an important aspect of type 0 – 3 CPCM is that the quality of the cement matrix significantly affects the CPCM quality after final moulding. Therefore, ensuring an optimal hydration quality of the cement matrix is an important prerequisite for the successful preparation of type 0 – 3 CPCM. The curing temperature and curing humidity significantly affect the hydration quality of the cement matrix, thereby influencing the final moulding effect of the CPCM. However, in most papers on type 0 – 3 CPCM, no clear requirements for curing conditions have been reported, and the hydration of the matrix phase materials is accelerated only by raising the curing temperature or increasing the curing humidity. A cement matrix with an optimal hydration degree and dense overall structure is beneficial for improving the efficiency of stress transfer to PZT particles through the matrix, thereby enhancing the piezoelectric properties of CPCM. Therefore, a study on the influence of the curing temperature and humidity on the final forming quality of CPCM is essential for obtaining the optimal forming conditions of CPCM, and the findings will serve as a reference for improving the yield of CPCM and the quality of finished products. In this regard, sulfoaluminate cement (SAC), with an acceptable hydration degree and a compact overall structure, can improve the efficiency of stress transfer to the functional phase through the matrix and enhance the piezoelectric properties of CPCM. Therefore, SAC was utilised as the base CPCM in this study. Existing studies have not strictly stipulated the size of type 0 – 3 CPCM. Therefore, in this study, a compromise scheme was adopted for the sample preparation process based on the existing research results, and samples were prepared with a diameter of 15 mm and thickness of 1 mm (Lu et al., 2015; Huang et al., 2009; Zhang et al., 2018; Kocherla et al., 2020; Pan and Huang, 2020). In view of the great potential of CPCM in the field of civil structure health monitoring, this paper aims to explore the best forming conditions of CPCM, and provide a meaningful theoretical reference for the application of CPCM in the field of civil structure health monitoring. In this study, the CPCM was maintained at different temperatures and humidity during experiments. The corresponding change in performance was tracked and tested at designated time nodes; the influence of temperature and humidity on the moulding process and quality of early CPCM was examined, and the optimal maintenance temperature, humidity, and time were further explored.

2. Experiments

2.1 Materials

The CPCM was composed of SAC as the matrix phase and PZT as the functional phase, with 0.3% added conductive carbon black

Table 1. Specific Parameters of PZT and SAC

	Specific gravity	Fineness	d_{33}	ε_r	K_t	g_{33}	$tg\delta$
PZT	7.2	/	600 pC/N	30,00	0.39	26×10^{-3} Vm/N	1.8
SAC	2.9	500 m^2/kg	/	/	/	/	/

(Pan et al., 2017). The specific parameters are listed in Table 1.

2.2 Sample Preparation

The volume ratio of PZT powder and SAC powder was controlled at 7:3, and 0.3% (mass fraction) carbon black powder was added to the aforementioned powders. Thereafter, distilled water was added to the mixture and stirred thoroughly. Subsequently, the mixture was added to a cylindrical mould (diameter: 15 mm), and the upper end was covered for hammer compaction to glue the aggregates, thereby ensuring the uniform material distribution in the mould before compaction. Subsequently, the static pressure was adjusted to 80 MPa for 2 min. After static pressing, the sample was taken out of the mould and placed in a curing environment with a pre-set temperature and humidity for more than 3 h, to ensure that the sample possessed a certain strength and satisfied the minimum requirements for polarisation. Thereafter, the sample was removed from the curing environment and placed in an oven (80°C) for 2 min for removing the surface moisture (Pan et al., 2017). Subsequently, the upper and lower surfaces of the sample were evenly coated with conductive silver glue, and the sample was heated again in the oven at 80°C for 2 min until the conductive silver glue was fully dried. Finally, the sample was placed on the mould for polarisation to obtain the CPCM sample, and the parameters of the polarised sample were measured.

The images of PZT before and after crushing and the mixture before and after compaction are presented in Fig. 1 The appearance and profile of CPCM are shown in Fig. 2.

Samples under different curing conditions were monitored at different time nodes. The specific conditions are presented in Table 2.

2.3 Polarisation and Measurement

The polarisation temperature of the sample should not be extremely high because the sample would heat up rapidly during polarisation. Furthermore, an extremely high temperature will lead to the loss of a large amount of crystalline water through heat evaporation, as displayed in Fig. 3.

To prevent the aforementioned issue, various factors must be

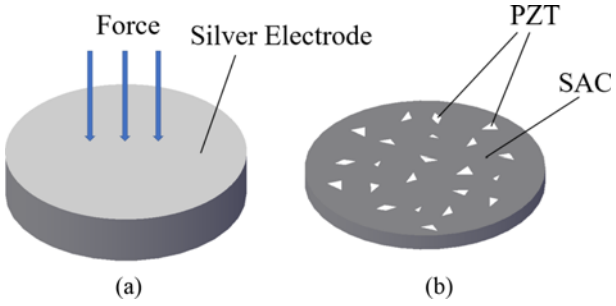

Fig. 2. CPCM Profile: (a) Overall Appearance of the CPCM, (b) CPCM Profile

Table 2. Curing Temperature, Curing Humidity, and Measuring Time Node

Curing temperature	20°C		50°C			80°C		
Curing humidity	40 RH		70 RH			100 RH		
Time node	6 h	9 h	12 h	18 h	24 h	36 h	48 h	72 h

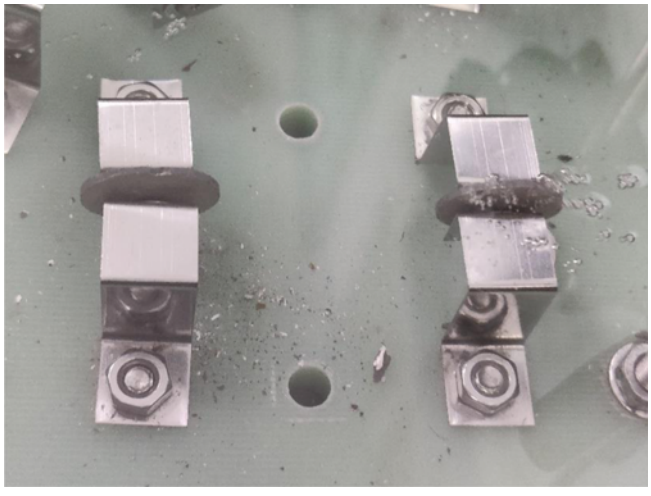

Fig. 3. Polarisation State: Fully Cured (left) and Uncured Specimens (right)

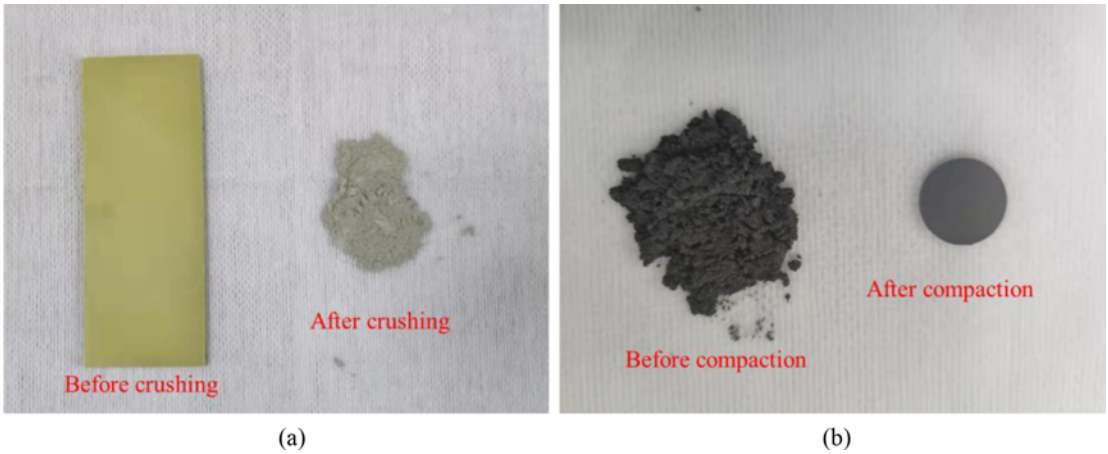

Fig. 1. PZT and PZT–SAC Mixture: (a) PZT before and after Crushing, (b) PZT–SAC Mixture before and after Compaction

investigated in detail.

2.3.1 Analysis of the Temperature Rise of the Sample During Polarisation

As PZT particles were dispersed in and closely connected to the SAC matrix, the temperature of the two components changed synergistically, and the rising temperature per unit time is calculated using Eqs. (1) and (2).

$$Q = c_P \cdot m_P \cdot T + c_S \cdot m_S \cdot T, \tag{1}$$

$$Q_I = \int_0^{t_0} i^2(t) \cdot R_p dt, \tag{2}$$

where T denotes the rising temperature of CPCM in the polarisation process; Q is the heat required to raise temperature T °C; c_P and c_S are the specific heat capacities of PZT and SAC, respectively; m_P and m_S are the quality of PZT and SAC, respectively; Q_I represents the polarisation process middle heat; $i(t)$ is the corresponding current at the moment of polarisation t; R_P is the equivalent resistance of CPCM at the moment; t represents the polarisation time of CPCM in an electric field; and t_0 represents the end time of polarisation (McLaren et al., 2019).

As the heating temperature of the CPCM originates from the electric heating energy generated during the polarisation process, the temperature change in the CPCM element can be expressed through Eq. (3), and the evaluation theorem of Eq. (4) can be leveraged to analyse the temperature calculation function.

$$T = \frac{R_P \int_0^{t_0} i^2(t) dt}{c_P \cdot m_P + c_S \cdot m_S}, \tag{3}$$

$$m(t_2 - t_1) \le \int_{t_1}^{t_2} f(x) dx \le M(t_2 - t_1), \tag{4}$$

where t_1 and t_2 correspond to the starting and ending points of the integral, respectively; $f(x)$ denotes the integrand; and m and M correspond to the valley and peak values in the defined interval, respectively. Herein, the following values were set: the smallest resistance $R_P = 3.93 \times 10^6\ \Omega$, $c_P = 0.42$ J/g, $m_P = 0.2284$ g, $c_S = 0.84$ J/g, and $m_S = 0.1781$ g. Consequently, when the polarisation current $i(t) = 0.1$ mA, the sample is heated by 4.8°C in only 30 s. Therefore, based on the calculation results and Eq. (4), the actual temperature of the sample increased by more than 4.8°C during the polarisation loading process. Moreover, even a small polarisation current can cause a large temperature increase in the CPCM, whereas the polarisation current of the sample at the initial hydration stage is considerably higher than 0.1 mA.

2.3.2 Analysis of the Loss of Crystal Water at High Temperatures

During the early stages of the test, in which the SAC hydration is incomplete, the process generates plasmas of OH^-, Ca^{2+}, SO_4^{2-} and Al^{3+} with free water, whereas the polarisation generates a weak current (Hunpratub et al., 2014). The main hydration products of SAC are $3CaO{\cdot}Al_2O_3{\cdot}3CaSO_4{\cdot}32H_2O$, $3CaO{\cdot}Al_2O_3{\cdot}CaSO_4{\cdot}12H_2O$, $Al_2O_3{\cdot}3H_2O$, and $CaO{\cdot}SiO_2{\cdot}H_2O$. These hydration products contain a considerable amount of water crystals, and an excessively high temperature can result in water crystal loss and reduced material properties. In particular, when the temperature is higher than 80°C, the linear relationship between the temperature and piezoelectric strain constant is no longer stable (Cheng, 2017; Wang et al., 2017). When the sample is not subjected to sufficient curing, the water readily evaporates and is lost because of the increase in the ambient temperature during polarisation.

Therefore, the polarisation process in this test is different from that of CPCM after complete hydration, and the polarisation temperature should be appropriately reduced. A moderate polarisation temperature of 60°C was selected to allow for the heating of the sample, and a low voltage of 100 V was applied as the initial voltage to prevent the generation of excessive polarisation current. After the current stabilised, the voltage and current changes were recorded, and the polarisation time was maintained at 15 min when the voltage reached 3 kV. Consequently, the polarisation current, polarisation time, piezoelectric strain constant (d_{33}), and equivalent resistance (R_P) of the CPCM were measured.

The relative permittivity ε_r is obtained using Eq. (5).

$$\varepsilon_r = \frac{C_P \cdot b}{\varepsilon_0 \cdot A}, \tag{5}$$

where C_P indicates the capacitance of the sample; b denotes the thickness of the CPCM element; the vacuum dielectric constant is presented as $\varepsilon_0 = 8.85 \times 10^{-12}$ F/m; and A depicts the cross-sectional area of the element. To ensure the accuracy of the test results, the average value obtained using three samples was reported.

3. Results and Discussion

3.1 Polarisation Voltage and Polarisation Current

In the first few hours following high-pressure CPCM moulding, the sample remained in a state of incomplete hydration and could not be polarised. The CPCM gradually formed a dense structure during the hydration process of the matrix, and therefore, the sample with complete hydration had less honeycomb cracks on the surface (Lu et al., 2015). The scanning electron microscopy (SEM) images enlarged by a factor of 1000 in Fig. 4 present the sample at the early hydration stage; several honeycomb cracks are observed, indicating that the crystallisation of the sample at the early hydration stage is not complete and that a complete and dense structure is not formed. After full hydration, the number of honeycomb cracks reduce. However, materials with an inadequately short curing time cannot meet the test requirements either in terms of strength or polarisation stability. Therefore, samples with a curing time of at least 6 h were selected for polarisation and measurement.

CPCM samples with different curing times were selected to monitor their polarisation process. The specific results are shown in Figs. 5 – 7. The polarisation of CPCM samples—with different curing times and under different curing conditions—was monitored

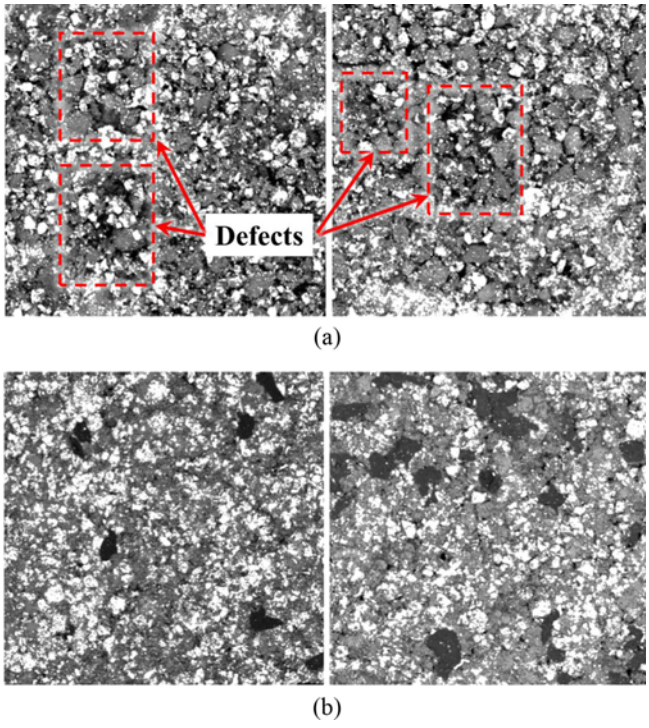

Fig. 4. SEM Scanning Images of Samples with Different Hydration Degrees: (a) Incomplete Hydration, (b) Complete Hydration

in this study, revealing that the curing temperature and humidity significantly influenced the polarisation process of the samples. Samples at 6, 18, and 72 h of curing were selected for measurement to concisely express the test results. The number represents the curing time; r indicates the real-time current when the voltage is loaded; and s denotes the current after stabilisation. For example, 72r represents the real-time current of the sample after curing for 72 h.

A high breakdown rate and low strength were observed at the initial curing stage for the sample prepared under low-temperature and low-humidity conditions. Furthermore, with an increase in the temperature, the hydration process was clearly accelerated, and the strength of the sample improved after the curing process. A comprehensive study of the data in Figs. 5 – 7 clearly indicates that the temperature and humidity conditions have a significant impact on the polarisation performance of the sample.

Further, the experimental results demonstrate that the current in the sample decreases with the progression of the polarisation process. The rate of current reduction generally reaches its maximum value at the initial stage of the external electric-field loading, and thereafter, it gradually decelerates. In addition, the maximum polarisation current of the sample with a short curing time can exceed 0.4 mA. However, with an increase in the curing time, the SAC matrix is gradually hydrated completely, and the

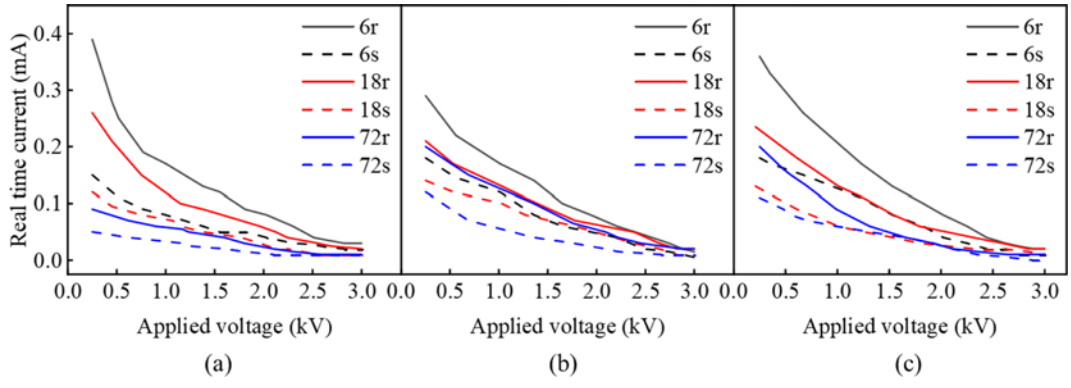

Fig. 5. Change in the Polarisation Current of the Sample at a Curing Temperature of 20°C: (a) 20°C/40 RH, (b) 20°C/70 RH, (c) 20°C/100 RH

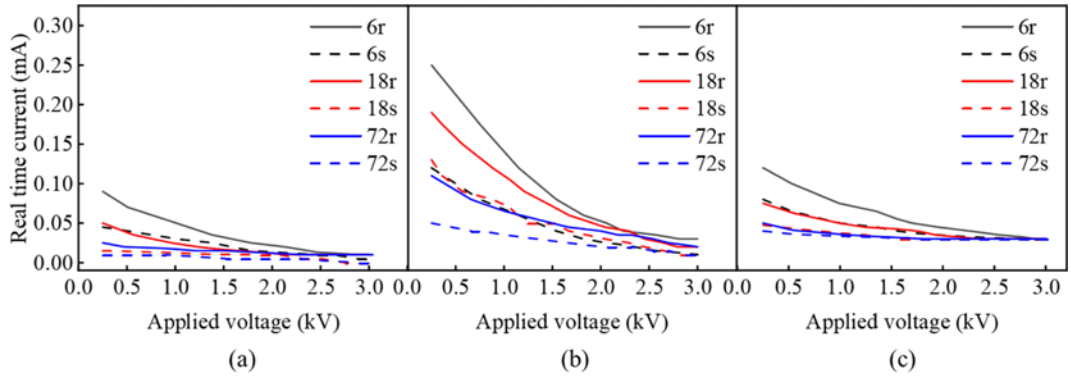

Fig. 6. Change in the Polarisation Current of Sample at a Curing Temperature of 50°C: (a) 50°C/40 RH, (b) 50°C/70 RH, (c) 50°C/100 RH

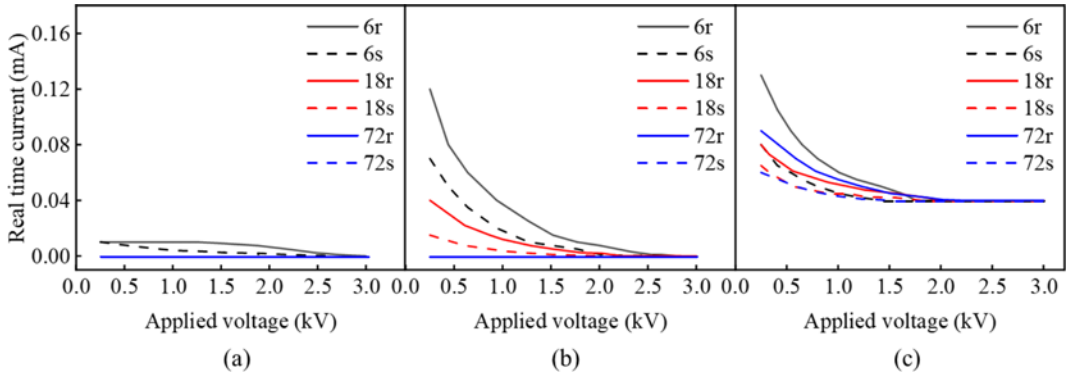

Fig. 7. Change in the Polarisation Current of the Sample at a Curing Temperature of 80°C: (a) 80°C/40 RH, (b) 80°C/70 RH, (c) 80°C/100 RH

CPCM structure becomes dense; consequently, the monitoring current decreases.

When the curing temperature is 20°C, the initial polarisation current of the sample at the initial hydration stage is large. In a certain range, the increase in the curing temperature can increase the participation of free ions in hydration, decrease the number of free ions, and minimise the resistivity per unit volume of cement slurry. From Figs. 5 – 7, a lower curing temperature results in the generation of a higher current in the sample during polarisation, regardless of the type of curing humidity. Moreover, with an increase in the curing temperature, the current generated during the sample polarisation process decreases significantly. Under the curing condition of 80°C/40 RH, after 18 h curing, the polarisation current of the sample stabilises at 0 mA.

Moreover, the analysis of the test results revealed that the curing humidity exerted a certain influence on the current in the CPCM during polarisation. For a curing humidity value of 40 RH, the higher the curing temperature, the earlier will the current attain a stable value during the process of polarisation. Consequently, for a curing condition of 20°C/40 RH, the polarisation current of the sample tends to be stable near the target voltage. In contrast, at 80°C/40 RH, the polarisation current of the sample stabilises at 0 mA at the initial loading stage. Further, when the curing humidity is 100 RH, the stable current of the sample at the target voltage increases with an increase in temperature. The stable currents at 20°C/100 RH, 50°C/100 RH, and 80°C/100 RH are 0, 0.03 and 0.04, respectively.

With an increase in the curing temperature, the difference between the initial polarisation current and the stable polarisation current exhibits a decreasing trend. Under the curing condition of 20°C/40 RH, the change in the polarisation current reaches 0.38 mA. However, at 80°C/40 RH and a curing time above 18 h, the current variation in the sample in the loading process is stable at 0. Therefore, the results show that the change in current during polarisation is determined by the curing temperature and humidity. Furthermore, in the range of 20 to 80°C, the increase in the curing temperature promoted the hydration process and improved the hydration rate of the CPCM. Therefore, the higher the curing humidity, the higher will be the final current when the polarisation attains the target voltage. Furthermore, the higher the curing temperature, the more stable will be the polarisation process and the smaller will be the current change.

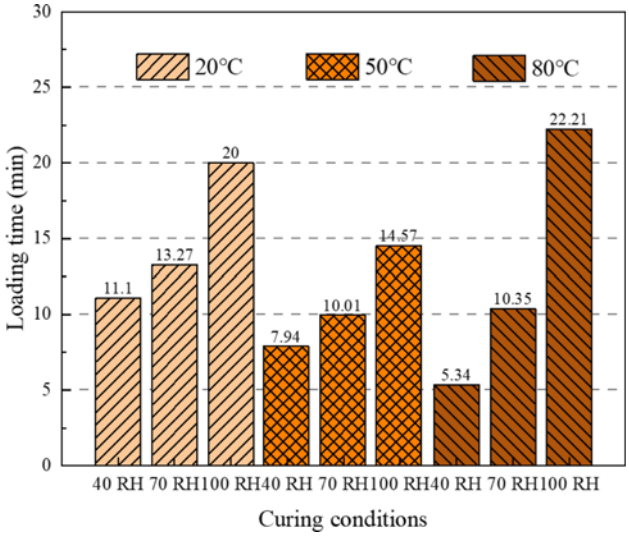

Fig. 8. Average Time to Reach the Polarisation Voltage under Different Curing Conditions

3.2 Loading Time

The influence of curing conditions on the polarisation efficiency of the sample was studied experimentally, and the average time required for the sample to reach the target voltage was recorded (Fig. 8).

The polarisation voltage was attained relatively faster for the sample cured under high-temperature and low-humidity conditions because the water molecules dissipated faster in the low humidity environment, thereby weakening the tunnelling effect of the CPCM during the polarisation process and hindering the formation of a conductive path. Compared with the samples cured at 20°C/40 RH and 50°C/40 RH, those cured at 80°C/40 RH attained the target polarisation voltage in a shorter time because the increase in temperature further accelerated the loss of water. In addition, with the increase in temperature, the hydration process of SAC was accelerated, thereby advancing the time of the exothermic peak of hydration. In contrast, the hydration rate of the matrix

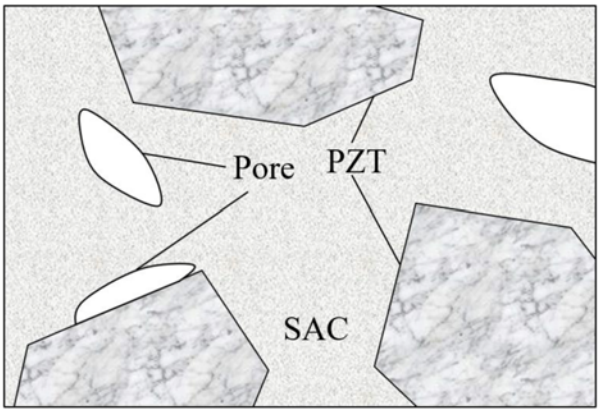

Fig. 9. Microscopic Schematic of the CPCM

material under the low-temperature curing condition was low, and a low loading rate was required during the voltage loading process (Zhang et al., 2020). At 80°C/40 RH, the polarisation time of the sample was the shortest among that of all analysed samples, owing to the coupling of low humidity and high temperature.

Under the curing condition of 80°C/100 RH, the loading time for the sample achieved the highest value among all groups. Essentially, the increase in temperature endows microscopic particles with a higher kinetic energy. Therefore, the curing conditions of high temperature and humidity enable the water molecules to acquire a higher kinetic energy and to participate more actively in the SAC forming process. Consequently, under the condition of the complete contact of hot and humid air, water molecules fill the pores of SAC and SAC-PZT (Fig. 9), thereby promoting the formation of conductive pathways in the sample. In addition, as illustrated in Fig. 7, when the curing condition is 80°C/100 RH, the stable polarisation current reaches 0.04 mA. However, to ensure that the sample does not disintegrate, additional time is required for the polarisation current to decrease to a stable value during the polarisation process. Therefore, under this condition, the voltage loading time is the largest among that of all groups. These results conclusively demonstrate that the increase in humidity is not conducive to the shortening of the polarisation time.

3.3 Equivalent Resistance Tracking and Monitoring

Over time, the ideal hydration of SAC material is gradually achieved, and the cement material undergoes the following three stages during the hydration process: dormancy, moulding, and maturity (Lu et al., 2015). In the SAC mixed with PZT particles, the particles in the initial composite do not possess a stable rigid connection with each other, and significant amounts of free salt ions and free water are present. However, with the hydration reaction, the SAC matrix skeleton begins to gradually form. Furthermore, the amount of hydration products continues to increase as the curing progresses, thereby filling the gaps in the matrix skeleton. Therefore, free water and free ions inside the sample are consumed, rendering the sample dense. This process continues, and consequently, the equivalent resistance of the

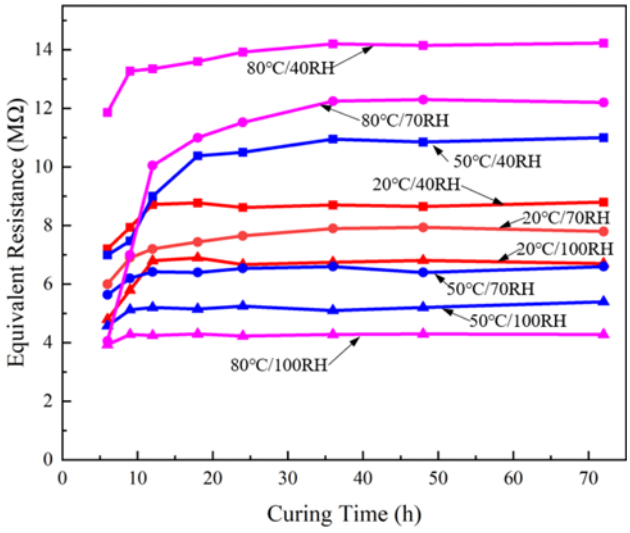

Fig. 10. Tracking and Monitoring of the CPCM Equivalent Resistance under Different Curing Conditions

material is closely related to its hydration process. The resistance of CPCM in different curing stages was tracked and monitored in the test. The results are plotted in Fig. 10.

The experimental results indicate that the resistance values of CPCM are significantly different under different curing conditions. A comparison of the samples at the same temperature revealed that the CPCM at the three curing temperatures of 20, 50 and 80°C reached the maximum and minimum resistances at 40 and 100 RH, respectively. Furthermore, when the humidity was 100 RH, the resistance value of the CPCM sample decreased significantly with increasing temperature and attained its lowest value under the curing condition of 80°C. In contrast, under the humidity condition of 40 RH, the resistance exhibited an increasing trend with the increase in temperature, reaching its maximum value at the curing temperature of 80°C.

When the curing temperature was 20°C, the stable resistance of CPCM exhibited a relatively minimal difference under different humidity conditions of curing, and the difference in the equivalent resistance value between 20°C/40 RH and 20°C/100 RH was within 3 MΩ. In contrast, at the curing temperature of 80 ?, the difference in the equivalent resistance between samples at 80 ?/40 RH and 80°C/100 RH exceeded 10 MΩ. Moreover, at the curing temperature of 50°C, the maximum difference in the stability resistance of the sample under different humidity conditions (i.e., between those at 20 and 80°C) was 5.6 MΩ. Overall, the resistance increased with the curing temperature after stabilisation because under low-humidity conditions, a higher temperature accelerated the dissipation of water, thereby weakening the hydrolysis of soluble salts and reducing the chances of conductive channel formation in the CPCM. Therefore, the higher the temperature, the more pronounced was the phenomenon. Moreover, with increasing humidity, particularly at 100 RH, the water molecules actively participated in the hydration of SAC in the high humidity environment, actively filling the pores of CPCMs owing to the kinetic energy endowed by the high temperature. Therefore, the

effect of water molecule loss was significantly weakened. Consequently, this further strengthened the formation probability of conductive paths in CPCM, thereby causing a more pronounced decrease in the resistance.

Notably, the increase in the curing humidity increased the time required to attain the resistance stability value. The CPCM reached resistance stability faster at a curing humidity of 100 RH than the samples under other conditions, and when the curing temperature was 80°C, the equivalent value of the sample was stable in the first 6 h because the SAC matrix had a higher probability of contacting water molecules during the hydration process in the high-humidity environment. Specifically, the increase in water accelerated the hydration rate of SAC, resulting in a more stable resistance. In contrast, under low-humidity conditions, the hydration rate decelerates owing to the reduction in the number of water molecules. Therefore, a higher humidity can shorten the time required by the material to reach the resistance stability value, whereas a lower humidity prolongs the hydration time of the material and decelerates the pattern-forming rate.

3.4 Piezoelectric Strain Constants

Under different curing conditions, the d_{33} value of the CPCM changes with increasing curing time, as illustrated in Fig. 11. The stabilisation of d_{33} can be accelerated by increasing the temperature. Under any humidity condition, more than 24 h were required to reach the stable relative dielectric constant at the curing temperature of 20°C. In contrast, a stable d_{33} value of the sample was achieved between the 12 – 18 and 9 – 12 h period at the curing temperatures of 50 and 80°C, respectively, indicating that the d_{33} forming period of the sample could be advanced by increasing the temperature appropriately. In addition, with the increase in temperature, the difference in the d_{33} value between 6 and 72 h gradually decreased because the sample began to hydrate after preparation, and the high temperature increased the hydration rate of SAC. Therefore, with the increase in the curing temperature, the degree of hydration reaction of the sample is higher. Therefore, the aforementioned results indicate that the curing temperature significantly influences the matrix phase SAC, and as a result, significantly influences the moulding rate of CPCM. Therefore, the moulding rate of the CPCM increases with the increase in temperature from 20 to 80°C.

The main hydration and heat release process of SAC at normal temperature is in the first 12 hours, and the hydration and heat release can be accelerated by properly raising the temperature. Furthermore, although the curing temperature does not affect the types of hydration products, it increases the number of hydration products (Wang et al., 2017). At a lower curing temperature, the d_{33} value after CPCM moulding did not exhibit any significant differences, whereas that for the sample prepared at 800°C clearly increased with increasing humidity. Under the curing condition of 80°C/100 RH, the d_{33} value exceeds 45 pC/N after curing for 9 h, which is approximately 1.5 times higher than that of the sample cured at 800°C/40 RH. However, for the curing temperatures of 20 and 500°C, the d_{33} value of the CPCM did not exhibit a significant change with the increase in the curing humidity. Therefore, these results indicate that the d_{33} value of CPCM is not significantly affected by humidity when the curing temperature is relatively low. The higher the humidity, the more pronounced is the increase in the piezoelectric strain constant of CPCM, indicating that the CPCM has a higher forming rate and higher piezoelectric strain constant at a higher curing temperature and humidity.

3.5 Relative Dielectric Constant

The relative permittivity is calculated using Eq. (4), and the results are presented in Fig. 12. The relative permittivity of CPCM samples is tracked and measured at different times. The results show that an increase in the temperature and humidity promotes an increase in the relative permittivity.

The stable value of the relative dielectric constant increases

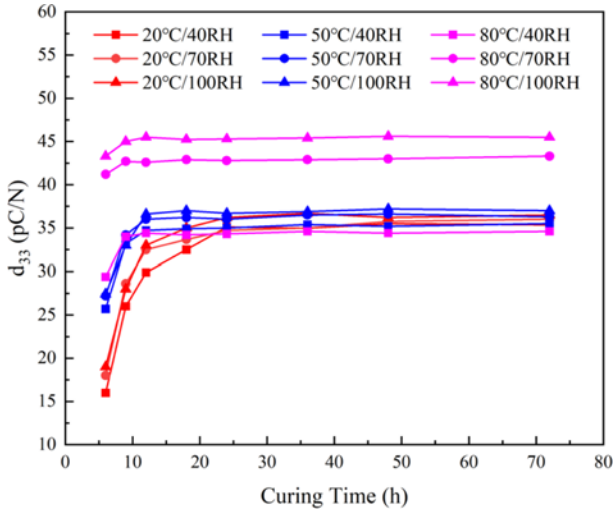

Fig. 11. Recorded Changes in the Piezoelectric Strain Constants with respect to the Curing Time

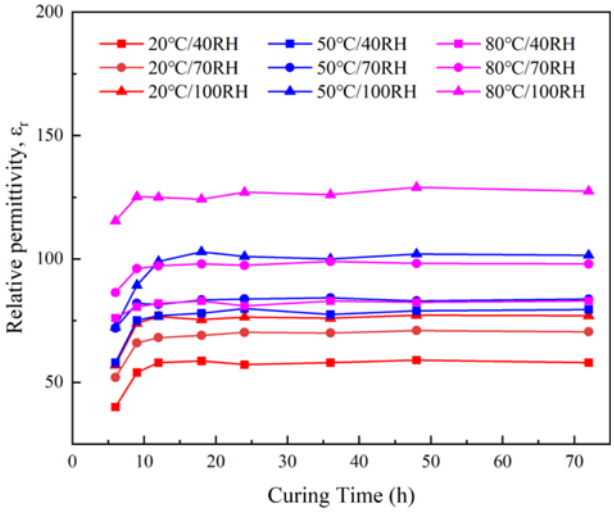

Fig. 12. Relative Dielectric Constant (ε_r) Varies with the Curing Time under Different Curing Conditions

with the curing temperature. Under identical humidity conditions, the relative permittivity of samples increases successively at curing temperatures of 20, 50, and 800°C. Furthermore, the relative dielectric constant of the CPCM increases from 76 at 200°C to 127 at 800°C when the curing humidity is 100 RH.

The CPCM performance under different curing humidity conditions was analysed; the relative dielectric constant of the CPCM increased significantly with increasing curing temperature. When the curing temperature is 200°C, the ε_r of the sample increases from 58.04 to 77.19, with an increase in humidity from 40 to 100 RH, respectively (representing an increase of 19.15). Consequently, this phenomenon is most pronounced at the curing temperature of 100°C, and the increase in ε_r, owing to the change in humidity from 40 to 100 RH, reaches a maximum value of 44.36.

The experimental results show that the relative dielectric constant of the sample is attributed to the coupled effect of the curing temperature and humidity. Therefore, for a curing temperature with a low humidity (80°C/40 RH and 80°C/70 RH), the relative permittivity of certain samples is close to or even lower than that of certain samples with a low curing temperature and high humidity (50°C/100 RH). Therefore, a low curing temperature and dry curing environment are not conducive to improving the relative dielectric constant of the CPCM, and the suitable curing environment should possess a high temperature and sufficient humidity.

4. Conclusions

Considering that CPCM is more suitable for health monitoring of civil structures than traditional piezoelectric materials and has great development potential in this field, this experiment tracked and recorded in detail the changes in five CPCM parameters, namely, the polarisation current, polarisation time, equivalent resistance, piezoelectric strain constant, and relative dielectric constant, at different curing temperatures and humidities with respect to the curing time. This study reveals the effect of different curing conditions on the performance of CPCM, provides an important reference for the efficient preparation of CPCM, and promotes the further production and application of CPCM in the field of civil structure health monitoring. Based on this study findings, the following conclusions were drawn:

1. A low curing temperature was not conducive for the preparation of CPCM. At the initial stage of polarization, the current of the sample at a curing temperature of 20°C was above 0.4 mA. However, with the increase in curing temperature, the forming speed of the sample accelerated, and the current in the loading process decreased. Subsequently, for a curing temperature of 80°C, the maximum current at the initial stage of polarization was only 0.12 mA. A higher curing temperature accelerated the specimen formation and significantly reduced the current during the polarisation process and improved the success rate of preparation.
2. The lower the curing humidity, the larger was the equivalent resistance value of the CPCM, and when the curing temperature was higher, the equivalent resistance of the CPCM was more susceptible to the influence of humidity. The equivalent resistance of the sample cured at 80°C/40 RH is 10 MΩ higher than that of the sample cured at 80°C/100 RH. In addition, when the temperature was low, the change of curing humidity resulted in a minimal change in sample resistance. When the curing temperature was 20°C, and the humidity was decreased from 100 to 40 RH, the equivalent resistance rise value was less than 3 MΩ.
3. Increasing the curing temperature can accelerate the stabilisation of the piezoelectric strain constant, and relative dielectric constant could be accelerated by increasing the curing temperature. At curing temperatures of 80, 50 and 20°C, the time required for the piezoelectric strain constant and the relative dielectric constant to reach stability was 9, 12 and 24 h, respectively.
4. A higher piezoelectric strain constant and relative dielectric constant was achieved by the CPCM under high-temperature and high-humidity curing conditions. At the same temperature, the piezoelectric strain constant and relative dielectric constant increased with increasing humidity. At the same humidity level, the piezoelectric strain constant and relative dielectric constant of the sample increased with increasing temperature. Further, both d_{33} and ε_r of CPCM reached maximum values of 45.6 pC/N and 127.47, at 80°C/100 RH, respectively.

Acknowledgments

This financial support is gratefully acknowledged, and the authors greatly appreciate the reviewer's comments, which have helped to improve the quality of the paper. This work was supported by the National Natural Science Foundation of China (Grant No. 51978534).

ORCID

Yu Rao https://orcid.org/0000-0003-4754-9175
Xiaoxiao Zhu https://orcid.org/0000-0002-1375-478X

References

Chai TT, Li ZW, Qin JM (2018) Application of piezoelectric ultrasonic sensor in the monitoring of concrete structure strain. *Journal of Nanoelectronics and Optoelectronics* 12(10):1093-1097, DOI: 10.1166/jno.2017.2233

Cheng X (2017) Cement-based piezoelectric composite and its application. Science Press, Beijing, China

Dong BQ, Li ZJ (2005) Cement-based piezoelectric ceramic smart composites. *Composites Science and Technology* 65(9):1363-1371, DOI: 10.1016/j.compscitech.2004.12.006

Dong BQ, Xing F, Li ZJ (2011) Cement-based piezoelectric ceramic composite and its sensor applications in civil engineering. *Aci Materials Journal* 108(5):543-549, DOI: 10.1016/j.researchgate.34957849

Gong HY, Li ZJ, Zhang YJ, Fan RH (2009) Piezoelectric and dielectric

behavior of 0-3 cement-based composites mixed with carbon black. *Journal of the European Ceramic Society* 29(10):2019-2019, DOI: 10.1016/j.jeurceramsoc.2008.11.014

Gong HY, Zhang YJ, Quan J, Chen SW (2011) Preparation and properties of cement based piezoelectric composites modified by CNTs. *Current Applied Physics* 11(3):653-656, DOI: 10.1016/j.cap.2010.10.021

Hou Y, Wang LB, Wang DW, Yang HL, Guo M, Ye ZJ, Tong XL (2017) A preliminary study on the IoT-based pavement monitoring platform based on the piezoelectric-cantilever-beam powered sensor. *Advances in Materials Science and Engineering* 2017:4576026, DOI: 10.1155/2017/4576026

Huang SF, Li X, Liu FT, Chang J, Xu DY, Chen X (2009) Effect of carbon black on properties of 0 − 3 piezoelectric ceramic/cement composites. *Current Applied Physics* 9(6):1191-1194, DOI: 10.1016/j.cap.2009.01.011

Huang SF, Ye ZM, Hu YL, Chang J, Lu LC, Cheng X (2007) Effect of forming pressures on electric properties of piezoelectric ceramic/sulphoaluminate cement composites. *Composites Science and Technology* 67(1):135-139, DOI: 10.1016/j.compscitech.2006.03.035

Hunpratub S, Yamwong T, Srilomsak S, Maensiri S, Chindaprasirt P (2014) Effect of particle size on the dielectric and piezoelectric properties of 0-3BCTZO/cement composites. *Ceramics International* 40(1):1209-1213, DOI: 10.1016/j.ceramint.2013.05.118

Kocherla A, Subramaniam KVL (2020) Embedded electrical impedance-based PZT sensor for monitoring hydrating concrete: Development and evaluation. *Smart Materials and Structures* 29(5):055038, DOI: 10.1088/1361-665X/ab6955

Lezgy-Nazargah M, Saeidi-Aminabadi S, Yousefzadeh MA (2019) Design and fabrication of a new fiber-cement-piezoelectric composite sensor for measurement of inner stress in concrete structures. *Archives of Civil and Mechanical Engineering* 19(2):405-416, DOI: 10.1016/j.acme.2018.12.007

Lim YY, Kwong KZ, Liew WYH, Soh CK (2017) Practical issues related to the application of piezoelectric based wave propagation technique in monitoring of concrete curing. *Construction and Building Materials* 152:506-519, DOI: 10.1016/j.conbuildmat.2017.06.163

Lu YY, Li ZJ, Liao WI (2011) Damage monitoring of reinforced concrete frames under seismic loading using cement-based piezoelectric sensor. *Materials and Structures* 44(7):1273-1285, DOI: 10.1617/s11527-010-9699-0

Lu YY, Ma HY, Li ZJ (2015) Ultrasonic monitoring of the early-age hydration of mineral admixtures incorporated concrete using cement-based piezoelectric composite sensors. *Journal of Intelligent Material Systems and Structures* 26(3):280-291, DOI: 10.1177/1045389X14525488

Lu YY, Zhang JR, Li ZJ, Dong BQ (2013) Corrosion monitoring of reinforced concrete beam using embedded cement-based piezoelectric sensor. *Magazine of Concrete Research* 65(21):1265-1276, DOI: 10.1680/macr.13.00071

McLaren CT, Kopatz C, Smith NJ, Jain H (2019) Development of highly inhomogeneous temperature profile within electrically heated alkali silicate glasses. *Scientific Reports* 9:2805, DOI: 10.1038/s41598-019-39431-8

Pan HH, Huang MW (2020) Piezoelectric cement sensor-based electromechanical impedance technique for the strength monitoring of cement mortar. *Construction and Building Materials* 254:119307, DOI: 10.1016/j.conbuildmat.2020.119307

Pan WH, Sun XD, Wu LM, Yang KK, Tang N (2019) Damage detection of asphalt concrete using piezo-ultrasonic wave technology. *Materials* 12(3):443, DOI: 10.3390/ma12030443

Pan HH, Wang CK, Cheng YC (2017) Curing time and heating conditions for piezoelectric properties of cement-based composites containing PZT. *Construction and Building Materials* 129:140-147, DOI: 10.1016/j.conbuildmat.2016.10.107

Qin L, Lu YY, Li ZJ (2010) Embedded cement-based piezoelectric sensors for acoustic emission detection in concrete. *Journal of Materials in Civil Engineering* 22(12):1323-1327, DOI: 10.1061/(ASCE)MT.1943-5533.0000133

Ruan XQ (2017) Investigation on early hydration behavior of cement based on piezoelectric sensor. *Emerging Materials Research* 6(1):184-188, DOI: 10.1680/jemmr.16.00138

Wang PM, Li N, Xu LL (2017) Hydration evolution and compressive strength of calcium sulphoaluminate cement constantly cured over the temperature range of 0 to 80 degrees. *Cement and Concrete Research* 100:203-213, DOI: 10.1016/j.cemconres.2017.05.025

Wang CH, Wang S, Gao ZW, Song Z (2021) Effect evaluation of road piezoelectric micro-energy collection-storage system based on laboratory and on-site tests. *Applied Energy* 287:116581, DOI: 10.1016/j.apenergy.2021.116581

Yang S, Wu B, Liu XC, Li MZ, Wang HY, He CF (2021) Piezoelectric impact energy harvester based on the composite spherical particle chain for self-powered sensors. *Sensors* 21(9):3151, DOI: 10.3390/s21093151

Zhang YH, Li TB, Feng WK, Xiong Z, Zhang G (2020) Effects of temperature on performances and hydration process of sulphoaluminate cement-based dual liquid grouting material and its mechanisms. *Journal of Thermal Analysis and Calorimetry* 139(1):47-56, DOI: 10.1007/s10973-019-08426-y

Zhang YH, Liu ZY, Ding F, Zhang WQ (2018) Effect of piezoelectric ceramic particles size gradation on piezoelectric properties of 0 − 3 cement-based piezoelectric composites. *Smart Materials and Structures* 27(8):085029, DOI: 10.1088/1361-665X/aad0be

Zhang C, Panda GP, Yan QX, Zhang WL, Vipulanandan C, Song GB (2020) Monitoring early-age hydration and setting of portland cement paste by piezoelectric transducers via electromechanical impedance method. *Construction and Building Materials* 258:120348, DOI: 10.1016/j.conbuildmat.2020.120348

Zhang SQ, Zhang YM, Li ZJ (2018) Ultrasonic monitoring of setting and hardening of slag blended cement under different curing temperatures by using embedded piezoelectric transducers. *Construction and Building Materials* 159:553-560, DOI: 10.1016/j.conbuildmat.2017.10.124

Zhou HJ, Liu YQ, Lu YY, Dong P, Guo BW, Ding WJ, Xing F, Liu TJ, Dong BQ (2016) In-situ crack propagation monitoring in mortar embedded with cement-based piezoelectric ceramic sensors. *Construction and Building Materials* 126:361-368, DOI: 10.1016/j.conbuildmat.2016.09.050